Study of runaway electron dynamics at the ASDEX Upgrade tokamak during impurity injection using fast hard X-ray spectrometry

A. Shevelev[1], E. Khilkevitch[1], M. Iliasova[1], M. Nocente[2,3], G. Pautasso[4], G. Papp[4], A. Dal Molin[2], S. P. Pandya[5], V. Plyusnin[6], L. Giacomelli[3], G. Gorini[2,3], E. Panontin[2], D. Rigamonti[3], M. Tardocchi[3], G. Tardini[4], A. Patel[7], A. Bogdanov[1], I. Chugunov[1], D. Doinikov[1], V. Naidenov[1], I. Polunovsky[1], ASDEX Upgrade Team[8], EUROfusion MST1 Team[9]

[1]*Ioffe Institute, St. Petersburg, Russia;*
[2]*Dipartimento di Fisica "G. Occhialini", Università di Milano-Bicocca, Milan, Italy;*
[3]*Institute for Plasma Science and Technology, National Research Council, Milan, Italy;*
[4]*Max-Planck-Intitut für Plasmaphysik, Garching bei München, Germany;*
[5] *Institute for Plasma Research, Bhat, near Indira Bridge, Gandhinagar 382428, India;*
[6]*Instituto de Plasmas e Fusão Nuclear, Instituto Superior Técnico, Universidade de Lisboa, 1049-001, Lisboa, Portugal;*
[7]*School of Liberal Studies, PanditDeendayal Petroleum University, Gandhinagar, India;*
[8]*See the author list of H. Meyer et al. 2019 Nucl. Fusion 59, 112014;* https://doi.org/10.1088/1741-4326/ab18b8
[9]*See the author list of B. Labit et al. 2019 Nucl. Fusion 59, 0860020;* https://doi.org/10.1088/1741-4326/ab2211

Abstract

To study the runaway electron (RE) dynamics during plasma discharge and develop scenarios for disruption mitigation, a hard X-ray (HXR) spectrometric system has been developed and commissioned at the ASDEX Upgrade tokamak (AUG). The diagnostic system consists of two high-performance spectrometers based on LaBr3(Ce) scintillation detectors supplied with advanced electronics and analysis algorithms. These spectrometers view the AUG tokamak chamber quasi-radially at the equatorial plane. The measurements were carried out in the RE beam generation regimes by injecting argon into a deuterium plasma. In the interaction of a developed RE beam with a heavy gas target, powerful bremsstrahlung flux is induced, reaching energy close to 20 MeV. The electron energy distributions were reconstructed from the measured HXR spectra by deconvolution methods. The experimentally obtained maximum RE energies at different discharge stages were compared with relativistic test particle simulations that include the effect of toroidal electric field, plasma collisional drag force, synchrotron deceleration force. It was observed that the electrons attain their maximum energies within 50-100 ms after the gas injection. It gradually decreases due to the drop in loop voltage, energy loss due to synchrotron radiation emission and collisions dissipation of energy with the background plasma. HXR measurements at the discharge with multiple deuterium pellet injections allowed observing the effects of plasma cooling and argon ion recombination after the pellet injections. Argon density in AUG plasma after Massive Gas Injection was estimated using HXR measurements.

1. Introduction

During the development of fusion reactors with magnetic confinement such as the ITER Experimental Reactor and the DEMO Demonstration Reactor, key technical and scientific challenges arise. In combination with excessive electromagnetic forces, radiation and thermal loads acting on the components of the first wall of the tokamak chamber, strong longitudinal (in the toroidal direction) electric fields are induced at the stage of discharge quenching. If these electric fields are large enough to overcome the dissipative effect of Coulomb collisions, they transfer plasma electrons to the regime of unlimited acceleration (the so-called "runaway" mode) [1,2]. Disruptions of a discharge in tokamaks are often the reason for the formation of populations of high-energy runaway electrons (REs). The control of the generation of runaway electrons in a tokamak plasma is a necessary condition for safe operation at large plasma facilities such as JET [3, 4] or ITER [5, 6]. According to the ITER requirements for diagnostic measurements, two parameters should be monitored in the reactor plasma: the maximum energy of REs and the current carried by them [5]. The maximum RE energy should be determined with an accuracy of 20% in the range up to 100 MeV. The current carried by the RE beam at the stage of discharge quenching must be determined with 30% accuracy. The time resolution for both parameters is 10 ms. The choice of tools for diagnosing the generation and evolution of a runaway electron beam in plasma and determining its parameters (energy distribution and current) is limited. Hard X-ray spectroscopy of hot plasma is one of the few methods that allow one to estimate the energy distribution of REs. The possibilities of RE diagnostics by the bremsstrahlung registration were demonstrated in measurements at small and medium size tokamaks Globus-M [7], HT-7 [8-10], FT-2 [11, 12], J-TEXT [13,14], COMPASS [15] and TUMAN-3M [16]. In these experiments, the spectra of bremsstrahlung generated by the interaction of REs with the materials of the tokamak plasma facing components were measured. However, data on the distributions of confined REs in the tokamak plasma are of greatest interest. HXR spectrometry allows analyzing bremsstrahlung and reconstructing the RE distribution using deconvolution methods. It is possible to carry out measurements in the sub-MeV, and MeV ranges through a relatively thick layer of steel without direct access to the plasma. An advantage of HXR spectrometry is estimating the number of REs in the plasma volume visible for detectors. HXR spectrometers signal the appearance of a RE beam in a short time from its generation. Spectrometric HXR measurements make it possible to estimate the current carried by runaway electrons, to trace the dynamics of RE acceleration, to study the factors influencing the RE distributions and to consider possible options for suppressing and dissipating a developed RE beam and mitigating its consequences.

However, as was shown in [17], if the detectors observe the plasma radially, that is, perpendicular to the direction of electron motion, due to the high anisotropy of bremsstrahlung radiation, it becomes impossible to detect radiation generated by electrons with energies above 35 MeV. In addition, the efficiency of gamma spectrometers decreases with increasing photon energy, which reduces the accuracy of the data provided by HXR plasma diagnostics for electron energies of several tens of MeV. The accuracy of the maximum energy measurement can be improved by using a spectrometer with a tangential line of sight. Also, in the presence of electrons with energies of several tens of MeV, the use of methods based on measuring synchrotron radiation in the visible (VIS) and infrared (IR) ranges can help. These methods have been implemented in the RE studies at the TEXTOR [18], DIII-D [19,20], HT-7 [8], EAST [21], J-TEXT [22], KSTAR [23], Alcator C-Mod [24], and AUG [25] tokamaks.

Observation of confined REs is possible on medium and large tokamaks such as DIII-D, ASDEX Upgrade (AUG), EAST and JET. At the DIII-D tokamak, to study the spatial and energy distribution of REs at the current plateau stage, a multi-detector array was developed that tangentially views a poloidal cross-section of the tokamak chamber [26]. At the JET tokamak, spectrometric HXR measurements were carried out both at the stage of current ramp-up and plateau [27-30] and in MGI (Massive Gas Injection) regimes at the current quench phase [3]. In the case of ITER tokamak, a Hard X-Ray Monitor is being designed [31] to detect confined REs in the first plasma scenarios, and Radial Gamma-Ray Spectrometers are being designed [17] to detect REs in a subsequent phase of the ITER plasma scenarios.

Experiments of RE generation and suppression, following the onset of plasma disruptions, are conducted in AUG to validate theoretical models, which can then be used to evaluate post-disruption levels of RE current and design RE mitigation schemes in larger devices, like ITER and DEMO [32]. To study the dynamics of runaway electrons during a plasma discharge, as well as to develop disruption mitigation scenarios, a HXR spectrometric system was developed consisting of two fast scintillation $LaBr_3$(Ce) spectrometers, which observe the camera of the AUG tokamak quasi-radially [33,34]. This article is devoted to the aspects of using HXR-spectrometric measurements provided by these spectrometers and to the analysis of RE dynamics based on the data obtained in experiments with gas injection into the AUG plasmas.

The paper is organized as follows. Technical specifications of spectrometers used in experiments at AUG is provided in Sections 2, and a reconstruction technique of the RE distribution function is briefly described in Section 3. Section 4 presents an estimation of injected impurity profile and runaway electron current using the spectrometers. Temporal evolution of observed maximum energy of REs and its comparison with simulation results are reported in Section 5. Conclusions drawn from the HXR measurements are presented in Section 6.

2. Instrumentation

The HXR spectrometric system for studying runaway electrons at the ASDEX Upgrade tokamak consists of two scintillation spectrometers based on small-sized $LaBr_3$(Ce) crystals. The first detector [33] is located in the bunker about 1 m behind the Bragg spectrometer and at a distance of approximately 7 m from the machine first wall. It views the plasma along a radial line of sight which makes an angle of 98 to the toroidal magnetic field in the plasma core. The spectrometer consists of a 25 mm x 17 mm (diameter x height) cylindrical $LaBr_3$(Ce) crystal coupled to an R6231 Hamamatsu photomultiplier tube (PMT) and is placed inside a soft iron shielding. The spectrometer is operated in the hard X-ray energy dynamic range up to about 30 MeV. The energy resolution) is 4% at the 662 keV ^{137}Cs line. A fast data acquisition system (400 MHz, 14 bit) based on the Advanced Telecommunication Computing Architecture (ATCA) framework is used to acquire data from the detector in the so-called “segmented” mode. A free running digitizer stores a segment of data whenever the input signal exceeds a predefined threshold. Each segment consists of 128 consecutive points and a time stamp that indicates when the threshold has been exceeded for time-resolved analysis of the data. A similar data acquisition mode has been used earlier for gamma-ray measurements at the JET tokamak [35].

The arrangement of both HXR spectrometers relative to the ASDEX Upgrade tokamak is shown in Figure 1. The location in Bragg's bunker for placing a HXR detector is not very good due to the small thickness of the bunker walls. Evaluations of the detector's protection against scattered

radiation showed that the fraction of scattered radiation in the measured spectrum is 10-15% and it does not significantly affect the determination of the maximum electron energy. However, at high energies, scattered radiation could significantly distort the shape of the electron distribution obtained during the measured spectra deconvolution. The number of electrons in the spectrum with energies > 5 MeV could be overestimated by a factor of 2–3.

To reduce the contribution of scattered quanta in the measured HXR spectrum and improve the reconstructions of RE distributions, a second spectrometer was installed behind the biological shielding of the ASDEX Upgrade tokamak. The spectrometer was named REGARDS (Runaway Electron GAmma-Ray Detection System) [34]. The detector module of the spectrometer consists of a $LaBr_3$(Ce) crystal with dimensions Ø25mm×25mm coupled to a Hamamatsu R9420-100-10 photomultiplier tube. The detector is placed in an external cylindrical magnetic shield made of soft iron. The detector views the tokamak chamber through a hole in the biological shield with a diameter of 70 mm. A 10 cm long lead collimator with a Ø10 mm is inserted into the hole.

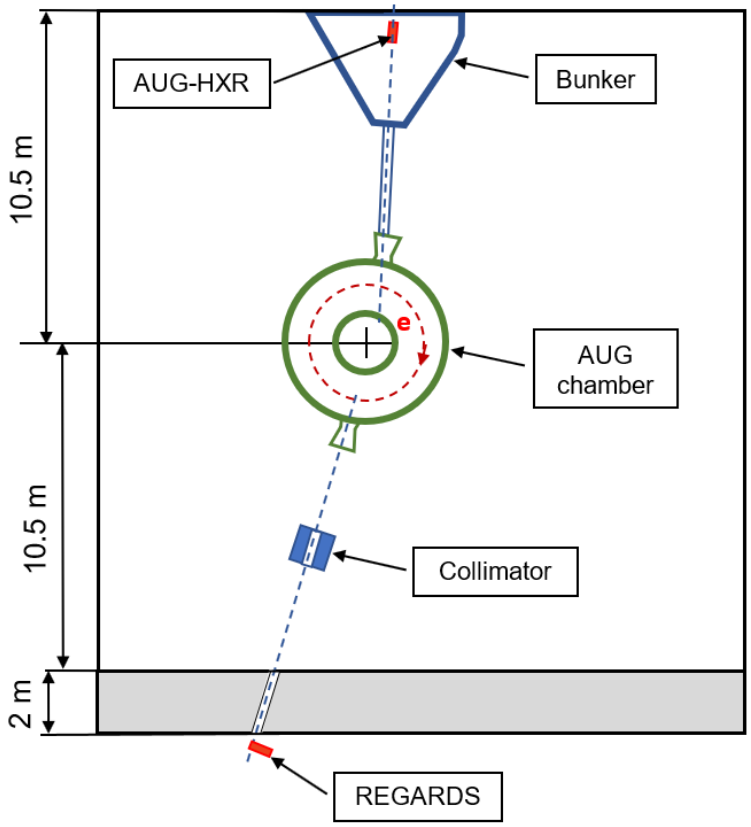

Figure 1 - Location of the HXR spectrometers near the tokamak chamber

The hardware of the data acquisition system of the REGARDS spectrometer includes an NI PXIe-1082 chassis, into which an NI PXIe-8840 controller, and an NI5772 (-02) ADC board with an NI PXIe-7966 FlexRIO module are inserted. The ADC board firmware developed using LabView tools provides operation with one channel at 800 MHz, 400 MHz, 200 MHz, 100 MHz sampling rate. Operation with two channels is possible at 400 MHz, 200 MHz and 100 MHz. Writing one ADC sample takes 2 bytes. For the purposes of collecting data from the $LaBr_3$(Ce) detector, the mode of operation with one channel at the maximum frequency 400 MHz, providing data collection without loss, was chosen.

The signal is transferred to the control computer PXIe-8840 embedded into the chassis, which records data to a solid-state drive (SSD). Signal recording initiated at the start signal and is performed for 10 or 20 seconds. For the entire AUG discharge, 8 GB or 16 GB of data is accumulated, respectively. Lossless compression of a digital signal before recording in real time using a two-pass coding algorithm was implemented using a software method. For storage, the signal is divided into successive blocks that are processed independently. The first pass uses double differential coding, which reduces the amount of stored data by about 2 times. For further compression, the Deflate (Huffman) algorithm applied to every second data block was used. This compression made it possible to further reduce the amount of data recorded to the disk by additional 15%. Thus, use of a NI PXIe-8840 control computer allows recording the detector signal for the entire discharge of the ASDEX Upgrade tokamak for 20 seconds at a data stream of 800 MB/s. The detector gain is monitored during the plasma discharge using a gain control system, which consists of an electrical pulse generator, a blue LED and an optical fiber. The pulse generator is used to run LED at a constant rate of 10 kHz. The light emitted by the LED and guided by an optical fiber to the photocathode of the PMT. During off-line analysis, the gain stability of the detector can be assessed by retrieving the LED pulses by pulse shape discrimination techniques and monitoring their relative magnitude. This system can be also used to correct small gain shifts.

3. Reconstruction of RE distribution functions

The RE distributions were reconstructed by deconvolution of the measured spectra using the DeGaSum [11, 27] code. The maximum likelihood estimation using expectation maximization (ML-EM) method [36-38] was implemented in the code. Application of the DeGaSum code based on the ML-EM for gamma-ray spectrum reconstructions is described in [27, 39]. During the deconvolution procedure, hard X-ray spectrum $y(\varepsilon)$ measured by the detector is represented in the convolution form

$$y(\varepsilon) = \int_0^\infty d\varepsilon' \, h_d(\varepsilon, \varepsilon') \int_0^\infty d\varepsilon'' \, h_e(\varepsilon', \varepsilon'') f(\varepsilon'') + n(\varepsilon), \qquad (1)$$

where ε, ε', ε'' – energies; $n(\varepsilon)$ – statistical noise; f - a runaway electron distribution function; h_d - a gamma-ray detector response function; h_e is HXR generation function, i.e. an energy-dependent density of probability for a bremsstrahlung emission produced by mono-energetic runaway electrons in the plasma volume of the detector field of view.

To reconstruct the RE energy distributions in the ASDEX Upgrade tokamak plasmas, Monte Carlo calculations of the detector response functions, bremsstrahlung generation in the tokamak chamber, and HXR transport toward towards the detector were carried out for both detectors. The calculations were conducted with MCNP6 code for what corresponding models have been developed. For the detector installed in the bunker behind the Bragg X-ray spectrometer the MCNP model included a detailed description of the detector with $LaBr_3$(Ce) Ø25mm ×17 mm crystal, photomultiplier tube and magnetic shield installed on the wooden shelf mounted on the wall behind the Bragg spectrometer. To verify the model conformity, the spectra of gamma-ray calibration sources Co-60 and Cs-137 have been reconstructed. For this purpose, a point gamma-ray source, located at 5.5 cm from the side surface of the crystal, was described in the model of the detector. Application of the DeGaSum code based on the ML-EM for gamma-ray spectrum

reconstructions is described in [39]. Gamma-ray spectrum y (ε) measured by a detector is represented as follows

$$y(\varepsilon) = \int_0^{+\infty} x(\varepsilon')h_d(\varepsilon, \varepsilon')d\varepsilon' + n(\varepsilon), \qquad (2)$$

where x is the initial gamma spectrum, h_d is the detector's instrumental response function, n is Poisson noise, i.e. Poisson distributed deviations, and ε - gamma-ray energy. Calculations of the detector response functions h_d were performed in the range of 0.1-2 MeV with the energy bin of 20 keV. Figure 2 shows the spectrum recorded by the spectrometer (after subtracting the natural gamma-ray background) and the original spectrum of the Co-60 source (1.173 and 1.332 MeV) reconstructed by the DeGaSum code.

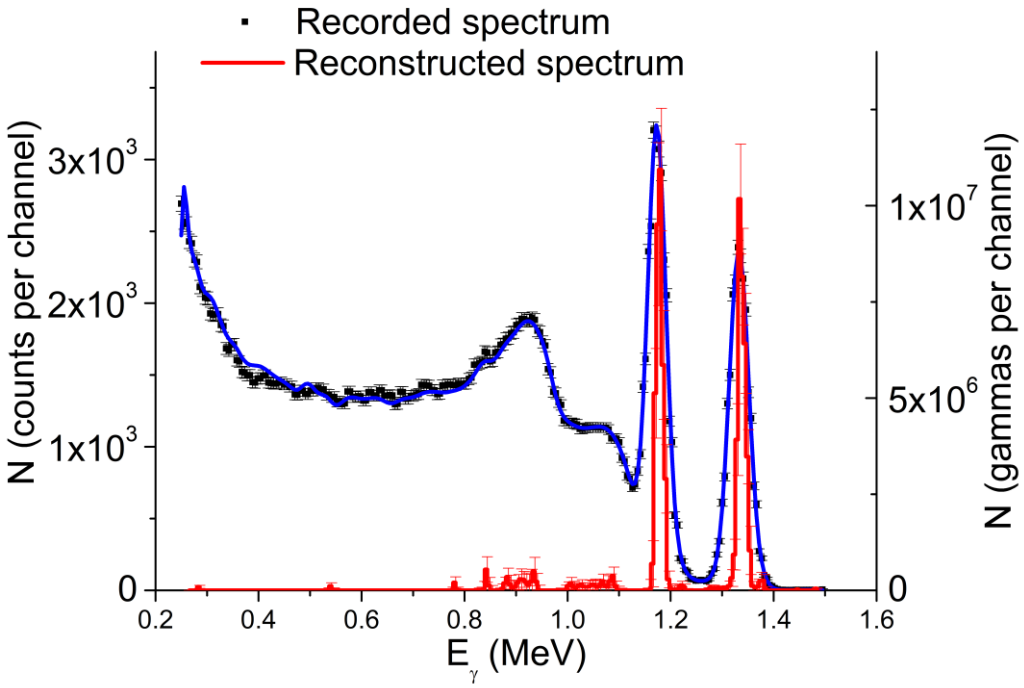

Figure 2 – Spectrum of Co-60 source recorded by the $LaBr_3$(Ce) spectrometer (black dots, left axis) and the result of the original spectrum deconvoluted by the DeGaSum code using the calculated response functions of the detector (red line, right axis). Blue line - convolution of the reconstructed spectrum with the detector response functions

The integral value of artifacts in the 0.35-1.1 MeV range is about 5%. These artifacts can be explained by the inaccuracy of the description of the source location in the model. To calculate transport of hard X-rays from the AUG chamber towards the detector detailed model of the Bragg spectrometer collimator has been developed.

For the REGARDS spectrometer the MCNP model includes the lead collimator of 10 cm in length and with Ø10 mm aperture placed in a hole in the of the AUG bioshield wall. The detector with Ø25mm ×25 mm crystal, PMT and the magnetic shield has its axis perpendicular to the collimator axis. Additional collimator made of polyethylene and lead blocks is installed in the AUG experimental hall [40]. For deconvolution of HXR spectra from AUG plasmas, response functions

h_d to the mono-energy gamma-rays were calculated in the range of 0.1–30 MeV with a step of 0.1 MeV for both detectors.

To obtain h_e functions, a few physical processes have been modelled in the MCNP considering the AUG vacuum vessel geometry and detector location. These processes are namely the interaction of mono-energetic RE electrons with Argon gaseous target of density 1×10^{20} m^{-3}, production bremsstrahlung emission and transport of the emission to the detector location including collimator and intervening materials. Since the bremsstrahlung generation cross-section is proportional to Z^2 of a target, the injected argon impurity makes the main contribution to the HXR emission and the presence of deuterium in the plasmas was ignored. In these calculations, a beam of monoenergetic electrons was simulated passing through a gas target in the volume of the tokamak chamber visible to the detector. Since the direction of motion of electrons in the beam is quasi-perpendicular to the direction of the plasma view, the calculations did not consider the pitch-angle distribution relative to the toroidal magnetic axis. The MCNP code was used to calculate the HXR distribution at the location of the crystals of both detectors in the energy range 0.1-30 MeV with a step of 0.1 MeV. Figure 3 shows examples of the response functions of the REGARDS spectrometer to monoenergetic gamma radiation and the bremsstrahlung distributions at the location of the detector crystal calculated for monoenergetic electrons.

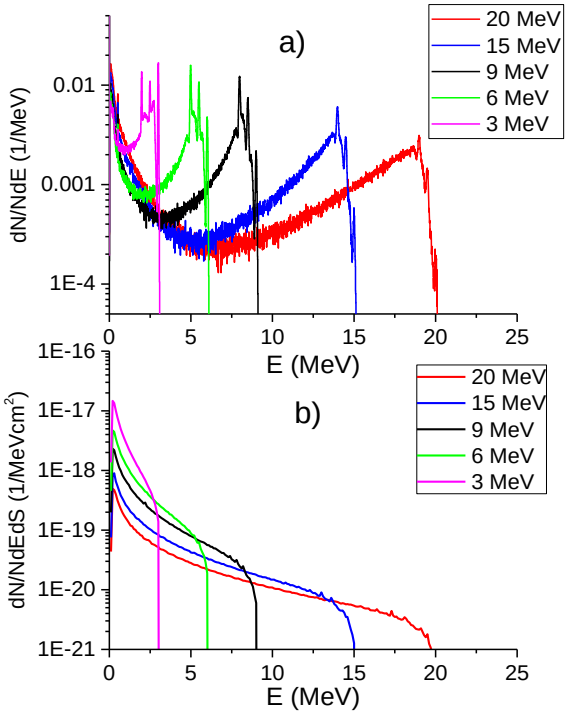

Figure 3 – Results of MCNP calculations: a) $LaBr_3$(Ce) detector response functions for 3, 6, 9, 15 and 20 MeV gamma-rays; b) bremsstrahlung distributions in the place of REGARDS installation corresponding to the interaction of mono-energetic 3, 6, 9, 15 and 20 MeV electrons with Argon

Figure 3a shows that the detector response function is continuous. The full energy peak and the peaks of annihilation quanta emission at high energies are weak. The bremsstrahlung functions in Figure 3b have a continuously decreasing form.

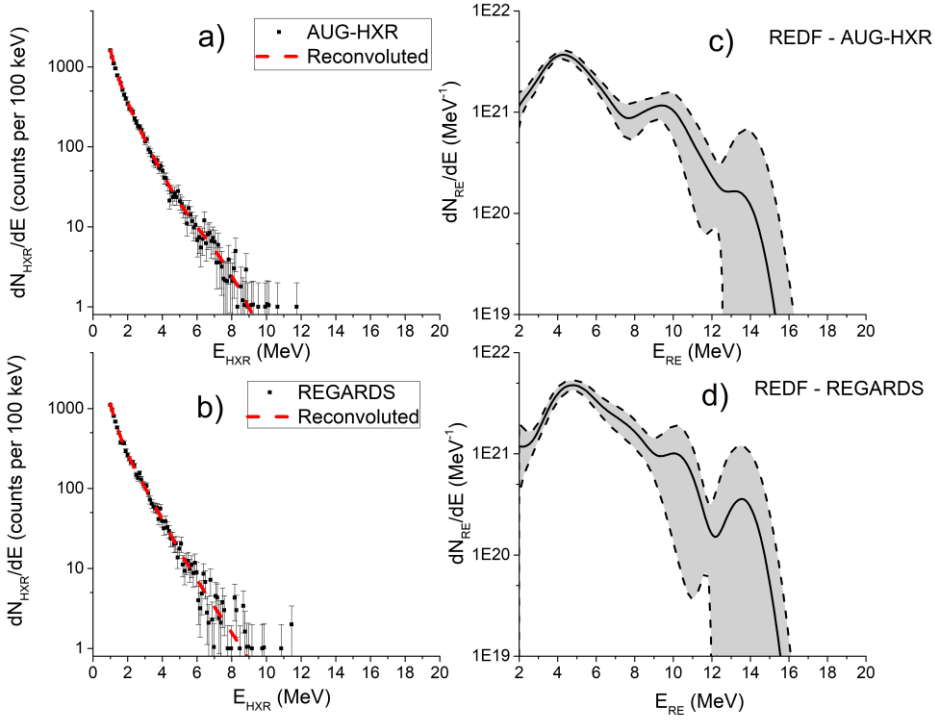

Figure 4 - Reconstruction of REDF from HXR spectra measured by AUG-HXR and REGARDS spectrometers during 1.03-1.06 s of the AUG discharge #36431: a) HXR spectrum measured by the AUG-HXR spectrometer (black dots); b) HXR spectrum measured by the REGARDS spectrometer (black dots); c) REDF reconstructed by the DeGaSum code from the AUG-HXR spectrum (4a); d) REDF reconstructed by the DeGaSum code from the REGARDS spectrum (4b)

In Figure 4, the HXR spectra recorded by the AUG-HXR (4a) and REGARDS (4b) spectrometers on 1.03-1.06 s of the AUG discharge #36431 are shown by black dots. In this discharge, RE beam was generated by argon injection on 1 s. Figures 4c and 4d show runaway electron distribution functions (REDF) reconstructed by the DeGaSum code from spectra 4a and 4b, respectively. The red dashed lines in Figures 4a and 4b show the results of convolution of the obtained REDFs with the detector response and RE generation functions according to formula (1).

4. Argon density evaluation

Runaway electrons were generated in AUG by injecting between 3×10^{20} and 4.8×10^{21} atoms of argon into low-density plasmas. The target plasmas had I_p = 0.7-0.8 MA, a low density (line averaged n_e = 2-4$\times10^{19}$ m^{-3}), a toroidal magnetic field B_t = 2.5 T and ~ 2.3 MW of ECRH input power; the plasma equilibrium was kept the same. R_0=1.61-1.63 m; a=0.55-0.56 m [32]. The addition of such a heavy gas as argon significantly increases accelerated electrons' energy loss due to scattering and radiation. To analyze RE acceleration dynamics, it is necessary to know the densities of the plasma components. The task is complicated because, first, the detectors observe a relatively small area of the plasma. The AUG-HXR detector observes approximately 10 cm of the plasma column in the vertical direction; for the REGARDS spectrometer, this value is about

15 cm. Second, at low energies E_{RE} < 1 MeV, spectrometers do not provide reliable data on the number of REs.

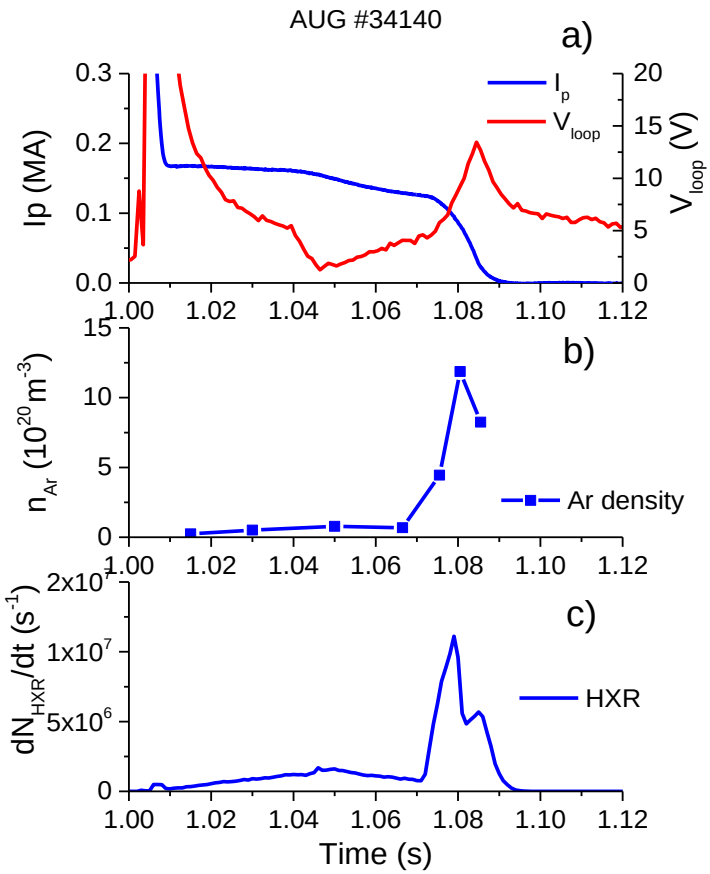

Figure 5 - Signals of discharge #34140: a) plasma current (blue line) and loop voltage (red line) after argon injection on t = 1 s of the discharge; b) argon density reconstructed from HXR measurements at the RE beam location visible to the AUG–HXR detector; c) time trace of the AUG- HXR spectrometer count rate

To estimate the fraction of REs visible to the AUG-HXR spectrometer, the signals recorded in discharge #34140 (see Figure 5) was analyzed. In this discharge, argon was re-injected for 1.07 s. Its assimilation, according to the analysis in [32], was 10%. Ionized argon could create an average density in the plasma, the volume of which on 1.07 s of the discharge was 3.5 m^3, about 6.6×10^{20} m^{-3}. The neutral argon density (90% of injected), evenly distributed over the chamber volume of 41 m^3, was 5.2×10^{20} m^{-3}. Thus, the argon's total density averaged over the plasma column was about 11.7×10^{20} m^{-3}. For this density of the argon target and for this time interval, the RE current was calculated from AUG-HXR measurements and processed with the DeGaSum code $I_{RE}=e\cdot N_{RE}/\Delta t$, where e is the electron charge; Δt is the spectrum acquisition time; N_{RE} is the number of electrons obtained after reconstructing the REDF f_{RE} with the DeGaSum code

$$N_{RE} = \frac{n_{Ar}^{m}}{n_{Ar}} \int_{\varepsilon_{min}}^{\varepsilon_{max}} f_{RE}(\varepsilon_{RE}) d\varepsilon_{RE} \qquad (3)$$

where n_{Ar}^{m} is the argon density used in the MCNP modelling, 10^{20} m^{-3}; n_{Ar} is real argon density; $\varepsilon_{max} = 30\ MeV$ -maximal energy of REs under consideration; $\varepsilon_{min} = 0.5\ MeV$ - minimal energy of REs under consideration. The repeated argon injection caused a sharp burst of hard X-

ray radiation, an order of magnitude higher than the radiation level's intensity before the second injection. The maximum emission occurred at 1.079 s of the discharge, 9 ms after the start of injection. Assuming that runaway electrons carry the entire plasma current, the RE current, the signal from which is recorded by the spectrometer, can be described as $I_{RE} = k_{det} \cdot I_p$, where k_{det} is a coefficient describing the fraction of REs visible for the spectrometer, taking into account the detection energy threshold, which was usually set at 0.5 MeV. For the AUG-HXR detector, this coefficient was found as $k_{det} = 0.37$.

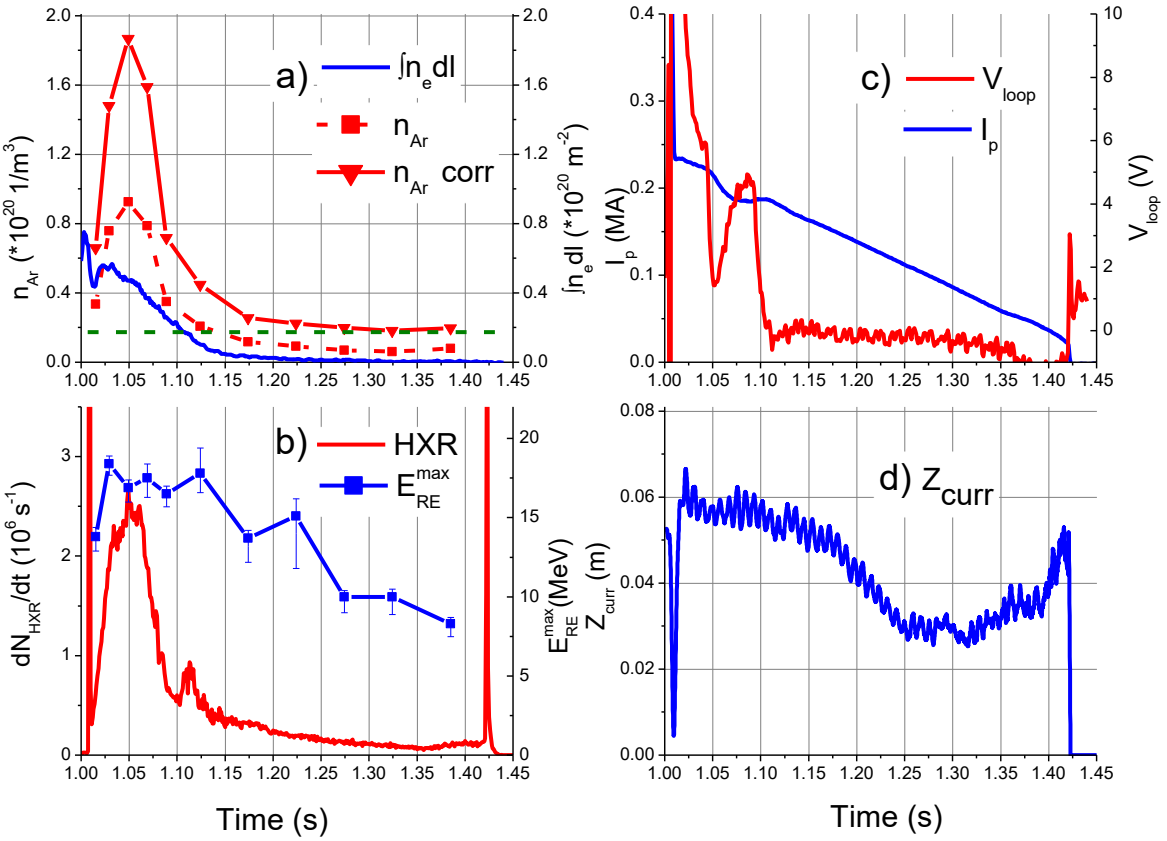

Figure 6 - Signals of the AUG discharge #34183: a) Line integrated electron density (blue line) and argon density assessed with HXR measurements for k_{det}=0.37 (red dashed line with dots) and for corrected k_{det}=0.12-0.18 (red line with dots). Green dashed line shows the density of injected argon uniformly distributed over the chamber volume; b) AUG-HXR detector count rate (red line) and obtained E_{RE}^{max} (blue line with dots); c) plasma current (blue line) and loop voltage (red line); d) Vertical position of plasma current relatively to the equatorial plane

The value $k_{det} = 0.37$ looks overestimated as AUG-HXR spectrometer has narrow plasma field of view. To correct k_{det} this value the discharge #34183 with series of D_2 pellet injection was processed. Figure 6 shows the signals recorded during this discharge. After the argon injection, which caused a RE beam generation with an initial current of 0.25 MA, 15 cryogenic D_2 pellets with a frequency of 70 Hz were injected into the plasma [32]. The pellets containing 5×10^{20} D_2 molecules each. The D_2 pellets carry a total of 1.5×10^{22} deuterium atoms, which, if uniformly distributed in a chamber volume of 41 m^3, gives a density of 3.7×10^{20} m^{-3}. The number of argon atoms injected to generate the RE beam is 7.44×10^{20}. A uniform distribution in the chamber

volume gives a density of 1.82×10^{19} m^{-3}. Using the value k_{det} = 0.37, the argon density evolution was obtained after processing the measured HXR spectra with the DeGaSum code. The n_{Ar} reaches a maximum at 50 ms after injection and is 0.93×10^{20} m^{-3}. If we take this value as an average over the plasma volume ~5 m^3, it corresponds to 62.5% of argon injected, which coincides with the estimating the argon fueling efficiency after the first injection, 60 ± 20%, provided in [32]. Then, during the D_2 pellet injection, a fairly quick decrease in argon density occurs, after which, from about 1.15 s of the discharge, the density changes weakly. Simultaneously, the density of free electrons becomes close to zero, which indicates the neutralization of the gas mixture in the tokamak. By 1.3 second of the discharge, argon density reaches a minimum, 0.6×10^{19} m^{-3}, which is noticeably lower than the assessment of the uniform distribution of argon over the tokamak chamber 1.82×10^{19} m^{-3} shown in figure 6a by green dashed line. The incorrect value of k_{det} could cause such a discrepancy. The value of k_{det} must be less by a factor of 3: ~0.12, for the obtained argon density at the end of the discharge to be equal to the uniformly distributed neutral argon concentration.

To correct the k_{det} value and study the influence of the RE beam size and position on the HXR flux coming to the detectors, MCNP simulations were conducted. The RE beam in the MCNP model had a circular cross-section with a Gaussian distribution of particles. Three distribution variants were considered: with the full width on half maximum (FWHM) of the electron flux 10, 15 and 20 cm. Realistic RE distribution obtained in one of AUG discharges with a maximum energy of ~ 19 MeV was used in the model. In the simulation, the HXR flux incident in the detectors was calculated at the position of the beam distribution center on the line of sight (displacement 0 cm) and vertical shifts of 2.5, 5, 7.5, 10, 12.5, 15, and 20 cm. The calculation results are shown in Figure 7. The HXR fluxes at the location of the spectrometer crystals were normalized to the flux from the RE beam with FWHM = 10 cm taken without displacement from LoS.

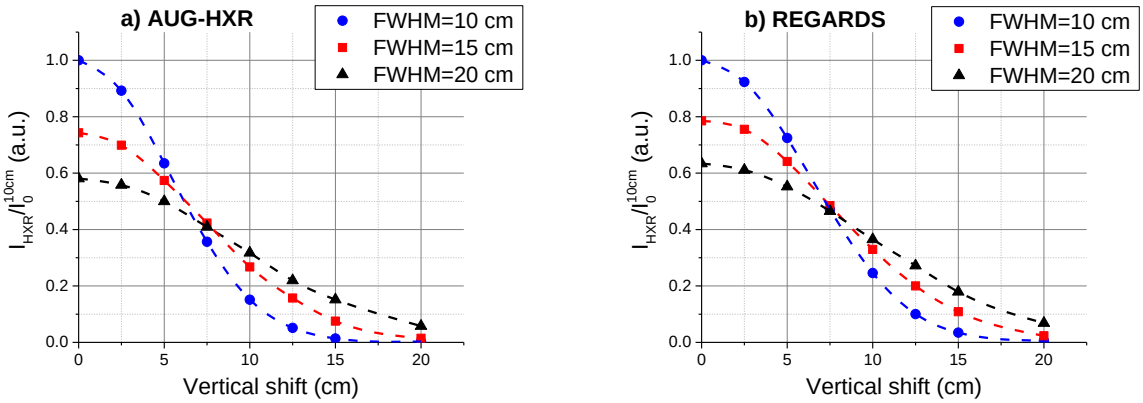

Figure 7 - Dependence of the HXR flux entering the detectors on the displacement of the electron beam with FWHM = 10, 15 and 20 cm relative to LoS of (a) AUG-HXR and (b) REGARDS

As can be seen in Figure 7, spectrometers are more sensitive to shifts of narrow beams. In general, the beam shifts relative to the equatorial plane were within 5-7 cm in the series of discharges with RE generation. In [25], the size and position of the RE beam in the AUG tokamak were analyzed by synchrotron radiation recorded by the camera in the visible light range. The diameter of the FWHM luminosity spot was approximately equal to $0.30\cdot a$ ~ 15 cm at 1.029 s of a discharge with

RE generation. The figure shows the evolution of the equilibrium of the electron beam during the discharge #34183 disruption.

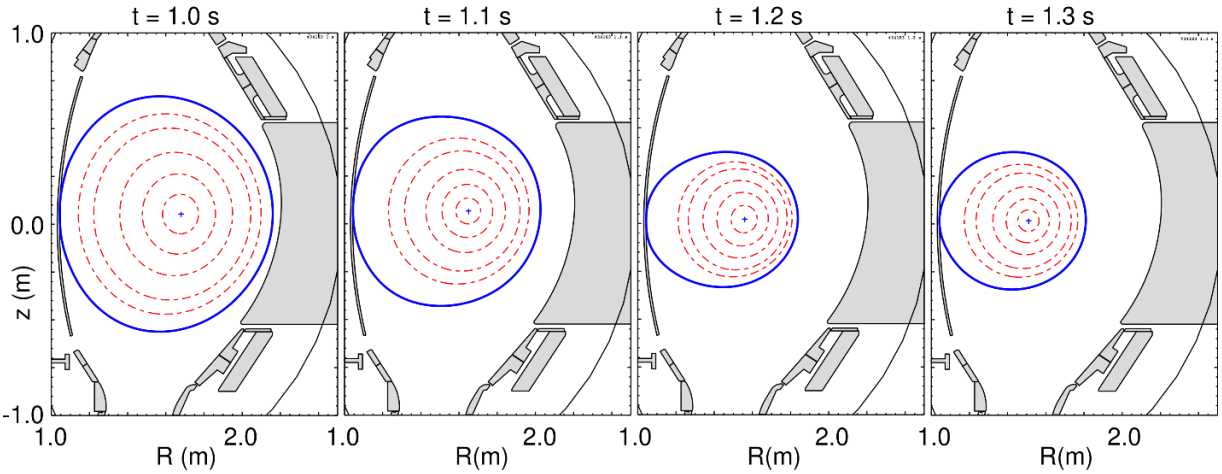

Figure 8 - Evolution of the RE beam magnetic equilibrium for AUG discharge #34183

Overall, the RE beam demonstrated a stable position. However, the maximum current-centroid shift relative to the position at the disruption beginning was ~ 3 cm at ~1.3 seconds of the discharge (see figure 6d). Considering the initial displacement of the beam relative to the observation axis of the spectrometer by 4 cm (AUG-HXR line of sight is by ~10 cm higher than the AUG equatorial plane), this could lead to a decrease in the number of electrons visible to the detector (coefficient k_{det}) by a factor of 1.5 at a beam size FWHM ~ 15 cm. Thus, the IR or VIS cameras registering synchrotron radiation and providing the size and position of the RE beam can supplement and correct the data supplied by HXR diagnostics on the magnitude of the RE current. Using the information on the RE beam position and size, we obtained the corrected value of k_{det}, which decreased from 0.18 at t=1.05 s to 0.12 at t=1.3 s due to the RE beam displacement. The resulted argon density evolution is shown in figure 6a by a solid red line with triangled dots.

The maximum value reached by argon to 1.05 s of the discharge is 1.87×10^{20} m^{-3}, which is by a factor of 2 higher than obtained previously 0.93×10^{20} m^{-3}. This discrepancy is explained by the fact that we assumed that in discharge #34140, ionized argon is uniformly distributed over the plasma volume; we did not know the exact value of the argon quantity but only assumed that it was ~ 10% of the amount injected the second time and did not consider the effect of the RE beam displacement on the HXR flux measured by the detector. As a result, we obtained a grossly overestimated k_{det} value. It is reasonable to assume that ionized argon is confined in the region of maximum RE current density. In this case, the average value of the argon density in the plasma volume keeps satisfying the ionization efficiency value of 60 ± 20%, provided in [32]. It should be noted that the plasma volume, as seen in Fig. 8, noticeably decreases during the RE current ramp down. It is also possible to change the size of the RE beam, which will affect the value of k_{det}. For a more accurate determination of the size and position of REs in future experiments, it is necessary to simultaneously measure HXR and synchrotron radiation in the IR/VIS range.

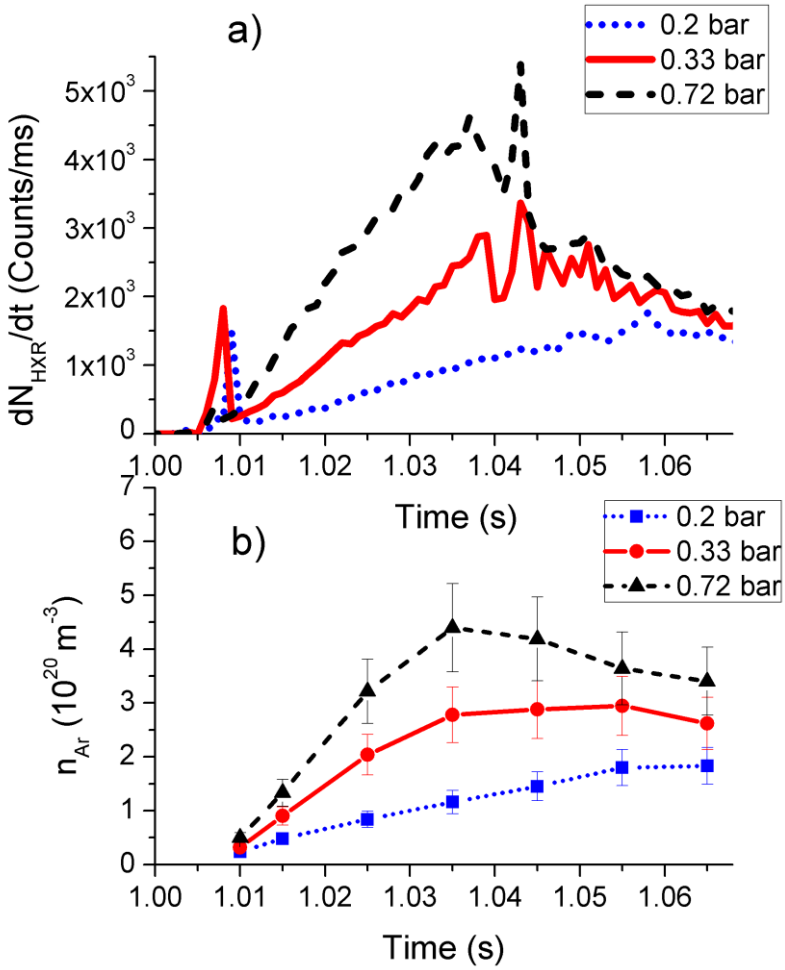

Figure 9 - AUG-HXR count rate (a) and argon density (b) evolution in the discharges with different amount of argon injected

Figure 9b shows the evolution of the density of argon interacting with the electron beam, reconstructed from the HXR flux measurements shown in Figure 9a. The density reconstruction was carried out starting from 10 ms after the argon injection. One can see that with an increase in the amount of injected argon, the HXR count rate increases proportionally and achieve a maximum more quickly, which indicates a more rapid increase in the density of the gas target. At 5-9 ms, HXR bursts are observed, which signals the release of electrons to the chamber wall, accompanying the MHD event. It is described in [42] that this MHD event seems to cause the accelerated penetration of argon into the central regions of the plasma column. Our observations confirm this: after the bursts, the HXR intensity rises rapidly and reaches a maximum at 35-55 ms after argon injection. At 10 ms after the injection of 0.72 bar of argon in discharge #34147, the observed argon density in the plasma center is ~ $5 \cdot 10^{19}$ m^{-3}, which is consistent with the modelling of argon penetration in discharge #33108 with a similar amount of injected gas conducted in [42].

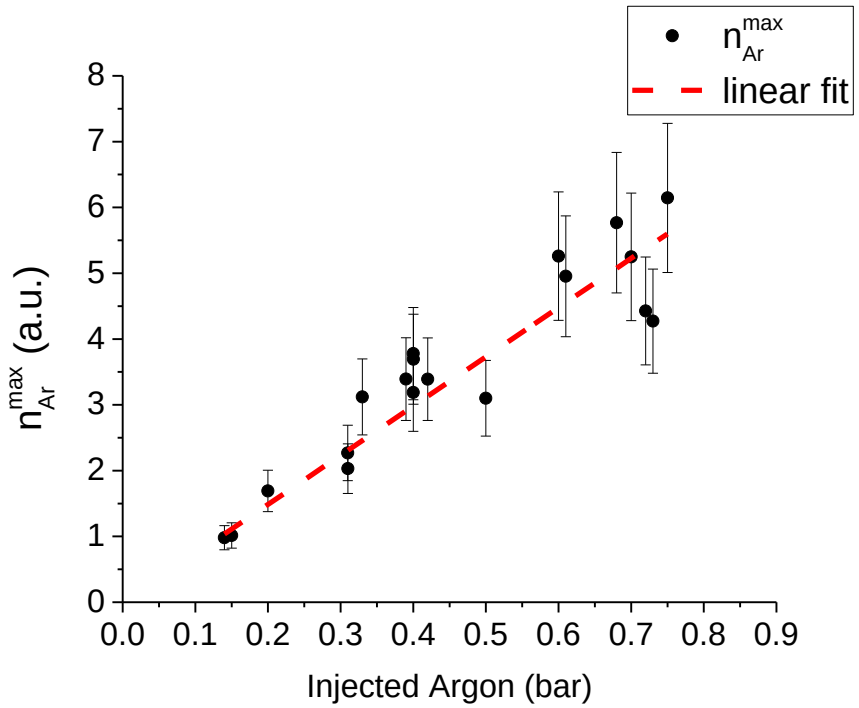

Figure 10 - Dependence of the maximum Ar density estimated using DeGaSum calculations vs injected argon value

HXR signals of 19 discharges with different amounts of injected argon were analysed. It was found that the maximum density of argon interacting with the RE beam is directly proportional to the amount of injected gas (Figure 10). This indicates a low contribution of radiation from the wall in the measured HXR spectra.

5. Evolution of RE maximum energy

An analysis of the RE acceleration in discharges with different values of injected argon was conducted. The evolution of Emax in discharge #34183, described above, is shown in Figure 6c by the red line. A series of injected pellets caused rapid recombination of argon, which resulted in a drop in the electron and argon densities in the place of the RE beam localization (Figure 6a).

A decrease in the gas density in the #34183 discharge should reduce the energy losses of accelerated electrons for collisions and bremsstrahlung, increasing the RE energy. However, from the moment the pellet injection began, the loop voltage dropped almost zero, which prevented further acceleration of electrons. In the discharge, the energy maximum was reached at 1.02–1.1 s, after which E_{RE}^{max} gradually decreases.

The experimental observations were investigated with numerical calculations performed to estimate RE energy dynamics using a simple 0-D code PREDICT [43, 44]. The code employs the relativistic test particle equations that govern RE energy dynamics in momentum space, including collisional and synchrotron-radiation induced losses [44-47]. It also considers different RE-generation mechanisms such as the secondary avalanche and primary RE-generation mechanisms, namely Dreicer, hot-tail, tritium decay and Compton scattering (from γ-rays emitted from activated walls) [46]. In the present simulation work, the following test particle equations utilized where the

effect of impurities are taken into account considering collisions of REs with free and bound electrons and scattering from the full and partially-shielded nuclear charge [46, 47]:

$$\frac{dp_{\|}}{dt} = eE_{\|} - \frac{e^4 m_e \alpha_e(\gamma)}{4\pi\varepsilon_0^2}\gamma(Z_{coll}(\gamma) + 1 + \gamma)\frac{p_{\|}}{p^3} - \left(F_{\mathrm{gc}} + F_{\mathrm{gy}}\frac{p_{\perp}^2}{p^4}\right)\gamma^4\beta^3\frac{p_{\|}}{p} \quad (4)$$

$$\frac{dp}{dt} = eE_{\|}\frac{p_{\|}}{p} - \frac{e^4 m_e \alpha_e(\gamma)}{4\pi\varepsilon_0^2}\frac{\gamma^2}{p^2} - \left(F_{\mathrm{gc}} + F_{\mathrm{gy}}\frac{p_{\perp}^2}{p^4}\right)\gamma^4\beta^3, \quad (5)$$

where $p_{||}$, $p_{\perp}$ and p are, respectively, the parallel, perpendicular and total electron momentum, $E_{||}$ is the toroidal electric field, γ is the relativistic gamma factor, $\beta = v_{RE}/c$, v_{RE} is the velocity of RE, and c is the speed of light. Here $F_{gc} = F_{gy}(m_e c\,/eB_T R_0)^2$, and $F_{gy} = 2\epsilon_0 B_T^2\,/3n_e\,m_e ln\Lambda$, are parameters describing the two contributions to the synchrotron radiation losses (the guiding center motion, F_{gc}, and the electron gyromotion, F_{gy}, respectively) [45]. m_e is the mass of an electron, ε_0 is the permittivity of free space. The parameters $\alpha_e(\gamma)$ and $Z_{coll}(\gamma)$ are correctional factors that take into account the collisions of REs with free and bound electrons as well as scattering from full and partially-shielded nuclear charge as calculated and described in [47]. In these simulations, all temporal evolution of plasma parameters has been taken as an input and the only free parameter is a temporal evolution of injected argon atoms density profile.

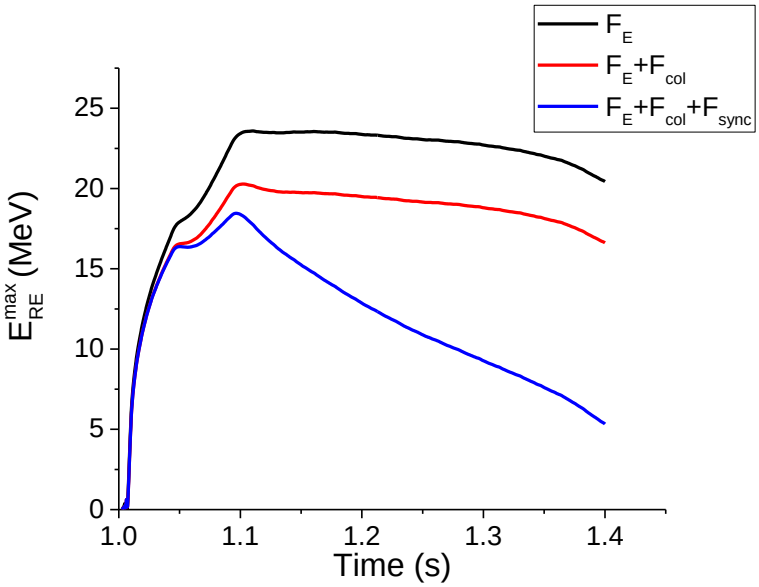

Figure 11 - Effect of different forces acting on the REs dynamics F_E (force due to electric field), F_{Coll} is force due to collisions of REs with plasma and impurity, ions and electrons, F_{syn} is synchrotron radiation loss

Figure 11 shows effect of different forces acting on the REs dynamics. For the early-born, high energy fraction of REs, the increase in perpendicular momentum enhances synchrotron losses significantly as compared to collisional losses. Hence, the presence of impurities has a two-fold effect on RE energy dissipation: the higher number of collisions decrease the RE energy and pitch-angle scattering of REs in presence of impurities also enhances synchrotron losses, especially for high energy REs.

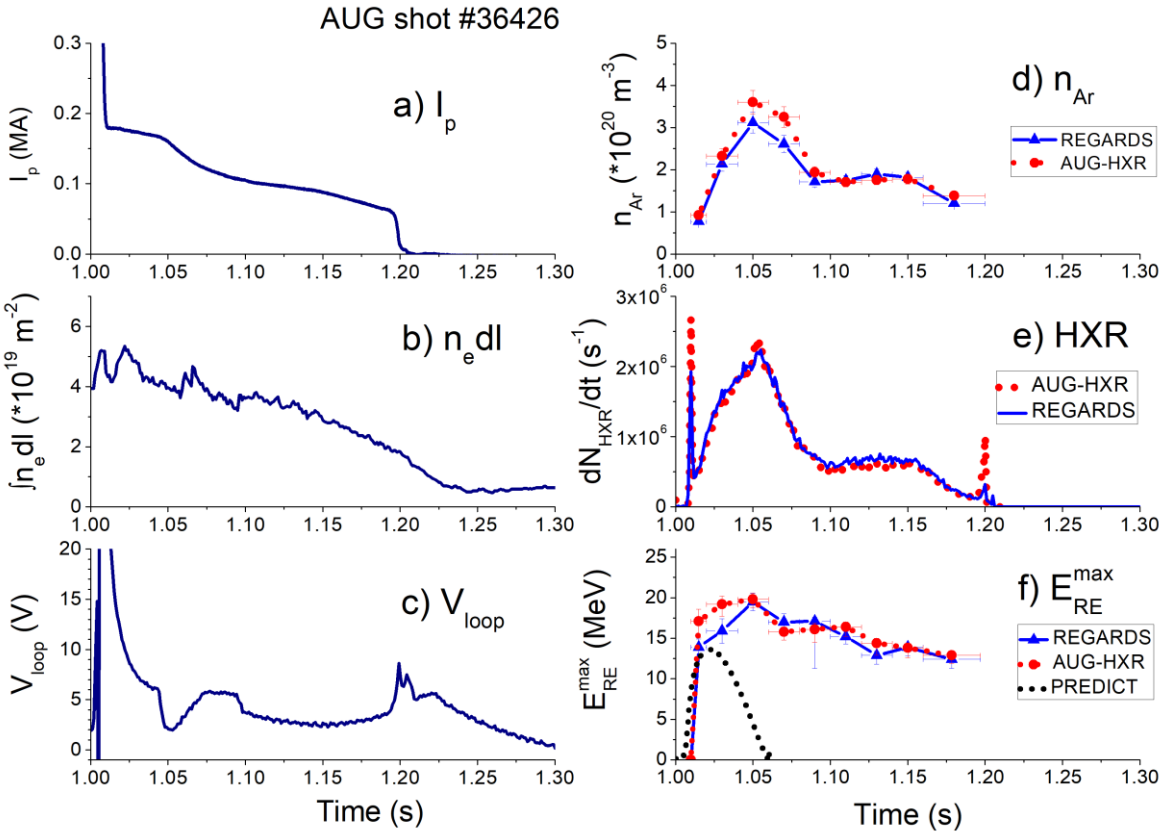

Figure 12 - Signals of discharge #36426: a) plasma current; b) linearly integrated electron density; c) loop voltage; d) argon density at the site of the RE beam localization, measured from the readings of the AUG-HXR spectrometers (red dots with a line) and REGARDS (blue dots with a line); e) count rate of the AUG-HXR spectrometers (red line) and REGARDS (blue line); f) E_{RE}^{max} obtained after signal processing of spectrometers (dots with lines) and the results of modeling the test particle method using n_{Ar} represented in Figure 9d (signal PREDICT, black line)

The signals of the #36426 discharge with RE generation caused by the injection of 9.6×10^{20} argon atoms are shown in Figure 12. Figure 12d represents the argon density evolution at the RE beam localization place in the AUG-HXR (red dots with a line) and REGARDS (blue dots with a line) spectrometer. Considering the correction for the shift of the RE beam from the detector's line of sight, the coefficient k_{det} varied in the range of 0.1-0.154. Whereas the REGARDS spectrometer sees ~ 15 cm of plasma column vs. ~ 10 cm for AUG-HXR, coefficient k_{det} for REGARDS varied in the range of 0.15-0.23. A slight difference in the found argon density for the detectors, in addition to possible unaccounted for errors, can be explained by a different volume of visible plasma. Similar time dependences of the detector counting rate shown in Figure 12e indicate a stable vertical position of the electron beam.

Analysis of the REDFs obtained from the deconvolution of the measured spectra using the DeGaSum code yielded the time dependence of the maximum RE energy shown in Figure 12f for both spectrometers. REs reach a maximum energy of 20 MeV 40-60 ms after argon injection, after which the electron energy gradually decreases to ~ 12.4 MeV due to collisions dissipation of energy with the background plasma. However, calculations carried out using the PREDICT code for this argon density gave significantly lower E_{RE}^{max} values (Figure 12f, black line). According to

these simulations, at a given argon density, the RE beam should disappear by 1.07 s of the discharge. Calculations with the PREDICT code showed that for the evolution of E_{RE}^{max} to correspond to the measured values, the argon density must be by order of magnitude lower than the values provided by HXR measurements. The possible reason behind the requirement of low Ar-density to explain the experimentally observed E_{RE}^{max} is attributed to several factors, namely a possible underestimation of N_{RE} in low energy range <0.5 MeV, contribution of pitch-angle that can enhance the bremsstrahlung radiation emission in the radial direction, interaction of REs with plasma walls, scattered photons registered by the spectrometers and faults in the test particle model corrected for RE interaction with impurity ions is exerting more drag force on REs that causing faster RE-energy dissipation. These possible reasons are under further investigation. Nevertheless, the present simulation results provide qualitative insight into RE-dynamics in the presence of impurity injection.

We analyzed the maximum RE energy dependence on the amount of injected argon in the range from 0.14 to 0.75 bar. E_{RE}^{max} was measured in 18 discharges in the time interval of 80–120 ms after argon injection. The resulting dependence is shown in Figure 13. In general, we cannot say that the amount of argon introduced in this density range significantly affects E_{RE}^{max}: its value decreases from about 18 to 16 MeV. We can also note the similarity in the E_{RE}^{max} evolution dynamics for discharges with different amounts of injected argon (Figure 13b). These observations require theoretical interpretations and the scope of our future study.

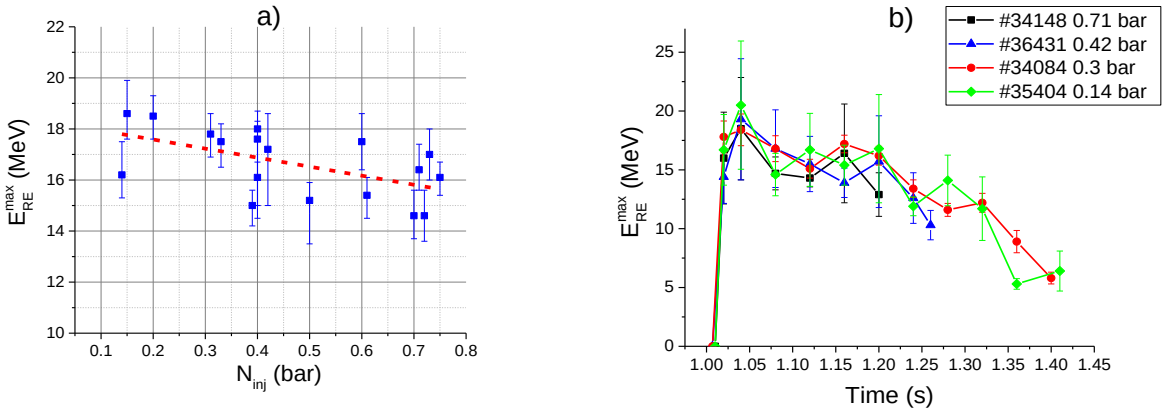

Figure 13 - E_{RE}^{max} observations at different Ar injections: a) E_{RE}^{max} dependence on the amount of injected argon. The red dashed line is the linear fit; b) E_{RE}^{max} evolution in discharges with different argon injections

It should be noted, that in recent measurements of synchrotron radiation carried out at AUG [25] using a fast visible camera Phantom V711 (having a narrow bend filter at 708.9 nm with FWHM of 8.6 nm), the presence of seed electrons with energies above 25 MeV was observed, while The HXR spectrometer for the same time interval gave a maximum energy of 16 MeV. The camera was configured in the runaway electron approach direction (tangential view) and utilized for the observation of the synchrotron emission and should start receiving the sufficient synchrotron emission signal once the REs gain energy more than 25 MeV with pitch angle 0.2 radian. The reasons for this discrepancy can probably be explained by the small number of

high-energy seed electrons in the plasma and the low sensitivity of the used HXR spectrometers to the radiation emitted at the perpendicular to the RE beam.

6. Conclusions

Two hard X-ray spectrometers based on small-size scintillation crystals $LaBr_3(Ce)$ were developed and put into operation at the ASDEX Upgrade tokamak. The spectrometers were used in experiments with the generation of REs in discharges with a low plasma density by injection of a small amount of argon. During the entire AUG discharge, the signal was recorded with a sampling rate of 400 MHz. For the pulse-height analysis of the recorded signal under conditions of a high spectrometer load with many piled-up pulses, the fitting method was used, making it possible to achieve a spectrometer count rate of 10^7 s^{-1} with a relatively low number of unresolved pulses. Analysis of the REDFs obtained from the deconvolution of the measured spectra using the DeGaSum code yielded the RE maximum energy time dependence. REs reach a maximum energy of 20 MeV 40-60 ms after argon injection followed with electron energy gradually decreases to ~ 12.4 MeV.

The obtained runaway electron distributions provided the assessments of the gas target's density and the RE beam fraction visible for spectrometers. The argon density coincides with argon fueling efficiency after the first injection, 60±20%, provided in [32] and the model of impurity ion transport into the central plasma considered in [42]. The RE maximum energy dependence on the amount of argon injected into the plasma was obtained, which was not significant: E_{RE}^{max} decreased by about 10% with an increase of injected argon from 0.14 to 0.73 bar. Test particle calculations carried out using the PREDICT code showed that for the evolution of E_{RE}^{max} to correspond to the measured values, the argon density must be by order of magnitude lower than the values provided by HXR measurements. The possible reasons behind the requirement of low Ar-density to explain the experimentally observed E_{RE}^{max} are under further investigation. Nevertheless, the present simulation results provide qualitative insight into RE-dynamics in the presence of impurity injection.

Performed measurement demonstrated the possibility of using small-sized spectrometers for diagnostics of runaway electrons in larger facilities such as ITER, where an HXR monitor system with crystals with similar characteristics is being developed. In the present study, the entire plasma current after argon injection was carried by runaway electrons, making it possible to estimate the argon density at the center of the plasma. In future experiments at ITER, it will be possible to solve the inverse problem of finding the RE current from the measured HXR signal, provided that the impurity distributions are known. For adequate estimation of the RE current, a spectrometric system with at least two plasma views in the field of observation of which the entire cross-section of the plasma column is located must be used. Measurement of synchrotron radiation in the IR/VIS ranges can supplement information about the size and position of the RE beam, as well as the presence of electrons with energies above 10 MeV.

ACKNOWLEDGEMENTS

This work has been carried out within the framework of the EUROfusion Consortium and has received funding from the Euratom research and training programme 2014-2018 and 2019-2020 under grant agreement No 633053. The views and opinions expressed herein do not necessarily

reflect those of the European Commission. RFBR, project number 19-32-90081, funded the work of Margarita Iliasova in the reported study. IST activities also received financial support from "Fundação para a Ciência e Tecnologia" through projects UIDB/50010/2020 and UIDP/50010/2020.

REFERENCES

[1] Driecer, H., Electron and Ion Runaway in a Fully Ionized Gas. I, Phys. Rev. **115** (1959) 238.
[2] Dreicer, H., Electron and Ion Runaway in a Fully Ionized Gas. II, Phys. Rev. **117** (1960) 329.
[3] Plyusnin, V.V., et al., Study of runaway electron generation during major disruptions in JET, Nucl. Fusion **46** (2006) 277
[4] Reux, C., et al., Runaway electron beam generation and mitigation during disruptions at JET-ILW, Nucl. Fusion **55** (2015) 093013.
[5] Donné, A. J. H., et al. Chapter 7: Diagnostics., Nucl. Fusion **47** (2007) S337.
[6] Helander, P., Eriksson, L.-G., Andersson, F. Runaway acceleration during magnetic reconnection in tokamaks, Plasma Phys. Control. Fusion **44** (2002) B247.
[7] Shevelev A. E., et al., Studies of runaway electrons in the Globus-M tokamak, Plasma Phys. Rep. 30 (2004) 159
[8] Chen Z. Y., et al., Measurement of the runaway electrons in the HT-7 tokamak, Review of Scientific Instruments 77 (2006) 013502
[9] S. Sajjad, et al., Runaway electron dynamics during impurity gas puffing on HT-7 tokamak, Physics of Plasmas 17 (2010) 042504
[10] Zhou R. J., et al., Effect of magnetic fluctuations on the confinement and dynamics of runaway electrons in the HT-7 tokamak, Physics of Plasmas 20,(2013) 032511
[11] Shevelev, A., et al., High performance gamma-ray spectrometer for runaway electron studies on the FT-2 tokamak, NIM A **830** (2016) 102–108
[12] Shevelev, A., et al., Runaway electron studies with hard x-ray and microwave diagnostics in the FT-2 lower hybrid current drive discharges, Nucl. Fusion **58** (2018) 016034
[13] Ma T.K., et al., Development of hard X-ray spectrometer with high time resolution on the J-TEXT tokamak, Nuclear Instruments and Methods in Physics Research A 856 (2017) 81–85
[14] Zhu X., et al., Observation of two threshold fields for runaway-electron generation in tokamaks, Nucl. Fusion 60 (2020) 084002
[15] Ficker O., et al., Losses of runaway electrons in MHD-active plasmas of the COMPASS tokamak, Nucl. Fusion 57 (2017) 076002
[16] Shevelev, A., et al., Study of runaway electrons in TUMAN-3M tokamak plasmas, Plasma Phys. Control. Fusion **60** (2018) 075009
[17] Finken K.H., et al., "Observation of infrared synchrotron radiation from tokamak runaway electrons in TEXTOR", Nuclear Fusion, Volume 30, Number 5, p859, (1990).
[18] A. Stahl, M. Landreman, G. Papp, E. Hollmann, and T. Fülöp, Synchrotron radiation from a runaway electron distribution in tokamaks, Physics of Plasmas 20, 093302 (2013);
[19] Yu J. H., et al., Visible imaging and spectroscopy of disruption runaway electrons in DIII-D Phys. Plasmas 20 (2013) 042113
[20] Zhou R. J., et al.,, Synchrotron radiation spectra and synchrotron radiation spot shape of runaway electrons in Experimental Advanced Superconducting Tokamak Physics of Plasmas 21, 063302 (2014);],
[21] Tong R. H., et al., Observation of runaway electrons by infrared camera in J-TEXT, Review of Scientific Instruments 87, 11E113 (2016);
[22] MunSeong Cheon, Dongcheol Seo and Junghee Kim, Observation of thermal quench induced by runaway electrons in magnetic perturbation, Nucl. Fusion 58 (2018) 046020

[23] TINGUELY, R. A., GRANETZ, R. S., HOPPE, M. & EMBRÉUS, O. 2018 Spatiotemporal evolution of runaway electrons from synchrotron images in Alcator C-Mod. Plasma Phys. Control. Fusion 60 (12), 124001
[24] Hoppe M., et al., Spatiotemporal analysis of the runaway distribution function from synchrotron images in an ASDEX Upgrade disruption, J. Plasma Phys. (2021), vol. 87, 855870102
[25] Paz-Soldan, C., et al., Spatiotemporal Evolution of Runaway Electron Momentum Distributions in Tokamaks, Phys. Rev. Lett. **118** (2017) 255002
[26] Shevelev, A., et al., Reconstruction of distribution functions of fast ions and runaway electrons in fusion plasmas using gamma-ray spectrometry with applications to ITER, Nucl. Fusion **53** (2013) 123004
[27] Shevelev, A., et al., Study of runaway electrons with Hard X-ray spectrometry of tokamak plasmas, AIP Conf. Proc. **1612** (2014) 125
[28] Plyusnin, V.V., et al., Comparison of runaway electron generation parameters in small, medium-sized and large tokamaks - A survey of experiments in COMPASS, TCV, ASDEX-Upgrade and JET, Nucl. Fusion **58** (2018) 016014
[29] Plyusnin, V.V., et al., Hard X-ray Bremsstrahlung of relativistic Runaway Electrons in JET JINST, **14** (2019) C09042
[30] Pandya, S.P., et al., Modeling of bremsstrahlung emission from the confined runaway electrons and applications to the hard x-ray monitor of ITER, Phys. Scr. **93** (2018) 115601
[31] Nocente, M., et al., Conceptual design of the radial gamma ray spectrometers system for a particle and runaway electron measurements at ITER, Nucl. Fusion, **57** (2017) 076016
[32] Pautasso, G., et al., Generation and dissipation of runaway electrons in ASDEX Upgrade experiments, Nucl. Fusion **60** (2020) 086011
[33] Nocente, M., et al., High resolution gamma-ray spectrometer with MHz capabilities for runaway electron studies at ASDEX Upgrade, RSI **89** (2018) 10I124
[34] Dal Molin, A., et al., "Development of gamma-ray spectrometers optimized for runaway electron bremsstrahlung emission in fusion devices", 46th EPS Conference on Plasma Physics (Proc. of 46th EPS Conference on Plasma Physics, Milan Italy, 2019) (2019) P1.1015
[35] Pereira, R.C., et al., ATCA data acquisition system for gamma-ray spectrometry, Fusion Eng. Des. **83** (2008) 341
[36] Vardi, Y., Shepp, L.A., and Kaufman, L., A Statistical Model for Positron Emission Tomography, J. of American Stat. Association **80** 389 (1985) 8–20
[37] Richardson, W. H., Bayesian-Based Iterative Method of Image Restoration, J. Opt. Soc. Amer. **62** 1 (1972) 55-59
[38] Lucy, L. B., An iterative technique for the rectification of observed distributions, Astron. J. **79** (1974) 745–754.
[39] Khilkevitch, E., et al., Application of Deconvolution Methods to Gamma-Radiation Spectra of Thermonuclear Plasma Tech. Phys. Lett. **39** 1 (2013) 63-67
[40] Tardini G., et al., First neutron spectrometry measurements in the ASDEX Upgrade tokamak, JINST **7** (2012) C03004
[41] Pandya, Santosh P., "Development and performance assessment of ITER diagnostics for runaway electrons based on predictive modelling", PhD thesis, AIXM0036, Aix-Marseille University, France, (2019) http://www.theses.fr/s194443
[42] Linder O., et al., Self-consistent modeling of runaway electron generation in massive gas injection scenarios in ASDEX Upgrade, Nucl. Fusion **60** (2020) 096031

[43] Patel, A., Pandya, S.P., "Simulation of runaway electron generation in fusion grade tokamak and suppression by impurity injection", 8th. PSSI-Plasma Scholars Colloquium (PSC-2020) 2020, KIIT University, Odisha, India (2021) https://arxiv.org/abs/2103.00325v1

[44] Martín-Solís, J. R., et al., Momentum–space structure of relativistic runaway electrons, Phys. Plasmas, **5** (1998) 2370

[45] Martín-Solís, J. R., et al., Runaway electron dynamics in tokamak plasmas with high impurity content., Phys. Plasmas **22** (2015) 092512

[46] Martín-Solís, J. R., et al., Formation and termination of runaway beams in ITER disruptions, Nucl. Fusion, **57** (2017) 066025

[47] Matsuyama, A., et al., Plasma and Fusion Research, Analysis of Avalanche Runaway Generation after Disruptions with Low-Z and Noble Gas Species, **12** (2017)1403032